Momentum distribution of 1D Bose gases at the quasi-condensation crossover: theoretical and experimental investigation

Thibaut Jacqmin, Bess Fang, Tarik Berrada, Tommaso Roscilde, Isabelle Bouchoule

▶ To cite this version:

HAL Id: hal-00716881

https://hal.archives-ouvertes.fr/hal-00716881v2

Submitted on 7 Nov 2012

Momentum distribution of 1D Bose gases at the quasi-condensation crossover: theoretical and experimental investigation

Thibaut Jacqmin[1], Bess Fang[1], Tarik Berrada[1,2], Tommaso Roscilde[3] and Isabelle Bouchoule[1]

[1] *Laboratoire Charles Fabry, Institut d'Optique, CNRS UMR8501,*
Université Paris XI, Avenue Augustin Fresnel, 91127 Palaiseau Cedex, France
[2] *Vienna Center for Quantum Science and Technology, Atominstitut, TU Wien, 1020 Vienna, Austria*
[3] *Laboratoire de Physique, CNRS UMR 5672, Ecole Normale Supérieure de Lyon,*
Université de Lyon, 46 Allée d'Italie, Lyon, F-69364, France
(Dated: November 7, 2012)

We investigate the momentum distribution of weakly interacting 1D Bose gases at thermal equilibrium both experimentally and theoretically. Momentum distribution of single 1D Bose gases is measured using a focusing technique, whose resolution we improve via a guiding scheme. The momentum distribution compares very well with quantum Monte Carlo calculations for the Lieb-Liniger model at finite temperature, allowing for an accurate thermometry of the gas that agrees with (and improves upon) the thermometry based on *in situ* density fluctuation measurements. The quasi-condensation crossover is investigated via two different experimental parameter sets, corresponding to the two different sides of the crossover. Classical field theory is expected to correctly describe the quasi-condensation crossover of weakly interacting gases. We derive the condition of validity of the classical field theory, and find that, in typical experiments, interactions are too strong for this theory to be accurate. This is confirmed by a comparison between the classical field predictions and the numerically exact quantum Monte Carlo calculations.

PACS numbers: 03.75.Hh, 67.10.Ba

I. INTRODUCTION

Correlation functions are essential to describe many-body systems. In particular, the first-order correlation function, or equivalently its Fourier transform, the momentum distribution, is an important observable, since it witnesses various phenomena such as the Bose-Einstein condensation transition, the Berezinskii-Kosterlitz-Thouless transition [1] or the Mott transition [2]. In the case of one-dimensional (1D) homogeneous gases, although one does not expect phase transitions, the correlation functions contain valuable information about the system. While the equation of state of 1D homogeneous Bose gases has been extensively studied in various regimes [3–6] and compared with exact theories [7], the momentum distribution has remained largely unexplored. It was measured for quasi-1D quasi-condensates using Bragg spectroscopy [8–10], and more recently it was investigated using the focusing technique for quasi-1D Bose gases in the crossover from the ideal Bose gas to quasi-condensate regimes [4, 11]. Density ripples that appear at the near field of a freely expanding quasi-1D quasi-condensate have also been studied [12, 13]. Although related to the second-order correlation function, they also provide information about the first-order correlation function within the quasi-condensate theory. The momentum distribution of an array of strongly correlated 1D Bose gases [14] constitutes the only measurement on a truly 1D system to our knowledge. From a theoretical point of view, the momentum distribution of 1D Bose gases with repulsive contact interactions is not known exactly over the entire phase diagram, but a few results have been established:

the mean kinetic energy can be extracted from the exact Yang-Yang thermodynamics [11], and the short-range correlations are responsible for a momentum tail scaling as $1/p^4$ [15–17]. The momentum distribution is known in the asymptotic regimes such as the ideal Bose gas and the quasi-condensate regimes, and a classical field approximation has been proposed to account for the crossover between them [11, 18–20].

In this work we investigate the momentum distribution of weakly interacting, purely or almost purely 1D Bose gases in various regimes around the quasi-condensation crossover. On the theory side, we find a criterion for the classical field theory [18, 19] to be accurate at the quasi-condensation crossover. Interactions are however too strong in our experiment to fulfill this criterion, and we implement exact Quantum Monte Carlo (QMC) simulations for the equilibrium behavior of the Lieb-Liniger model. We find that the measured momentum distribution agrees very well with QMC calculations. Moreover, the temperature extracted from a fit of the momentum distribution to the QMC calculations is in agreement with that obtained from *in situ* density fluctuation measurements [3, 6].

This paper is organised as follows. In Sec. II we recall the classical field approximation and investigate the conditions under which it is valid to describe the quasi-condensation crossover. We show that, in most experimental situations, the gas is too strongly interacting for this description to be accurate. We then present our QMC calculations, and compare them with the classical field prediction in the asymptotic limit. In Sec. III, we describe the experimental setup and the focusing technique we use to measure momentum distribution. We

discuss how we improve the resolution of this technique by means of a guiding scheme. In Sec. IV, we present our experimental results that span both the quasi-condensate regime (purely 1D) and the degenerate ideal Bose gas regime (almost 1D), and compare them to QMC results. We conclude and discuss the prospective work in Sec. V.

II. THEORETICAL PREDICTIONS

A. Model Hamiltonian and exact solution

We consider a 1D homogeneous Bose gas with repulsive contact interactions, described by the Lieb-Liniger Hamiltonian, whose grand-canonical expression is

$$\hat{H} = \int dz \left[-\frac{\hbar^2}{2m} \hat{\Psi}^\dagger \frac{\partial^2}{\partial z^2} \hat{\Psi} + \frac{g}{2} \hat{\Psi}^\dagger \hat{\Psi}^\dagger \hat{\Psi} \hat{\Psi} - \mu \hat{\Psi}^\dagger \hat{\Psi} \right], \quad (1)$$

where z is the position, $\hat{\Psi} \equiv \hat{\Psi}(z)$ is the field operator, g is the coupling constant, m is the mass of one boson and μ is the chemical potential. The thermal equilibrium state of the system is completely characterised by the density ρ and the temperature T, or by the dimensionless interaction parameter, $\gamma = \frac{mg}{\hbar^2 \rho}$, and the reduced temperature, $t = \frac{2\hbar^2 k_B T}{mg^2}$. The phase diagram [3] in the parameter space (γ, t) is given in Fig. 1, where lines should be understood as crossovers. In this article, we focus on the quasi-condensation crossover, which occurs, for $\gamma \ll 1$, around the line $\gamma_{co} = t^{-2/3}$ (solid line). The Lieb-Liniger model has the remarkable property of being integrable, giving access to exact results valid over the entire phase diagram. For example, the equation of state is known exactly through the Yang-Yang theory [7]. Yet, the calculation of the first order correlation function $g^{(1)}(z) = \langle \hat{\Psi}^\dagger(z) \hat{\Psi}(0) \rangle$ from the Bethe-Ansatz solution for finite γ and at finite temperature is still a subject of active research. Approximate analytic theories for the correlation functions exist in the limiting cases of ideal Bose gas regime (where the ideal Bose gas theory applies) and quasi-condensate regime (where the Bogoliubov theory applies [17]). However, the behavior of $g^{(1)}(z)$ at the crossover between those two regimes lacks a quantitative description.

B. Classical field theory

The full quantum many-body problem of Eq. (1) is notoriously complex. However, since thermal fluctuations are expected to dominate at the quasi-condensation crossover, it seems appropriate to simplify the problem using a classical field approximation, where the quantum field operators $\hat{\Psi}(z)$ and $\hat{\Psi}^\dagger(z)$ are replaced by the complex fields $\Psi(z)$ and $\Psi^*(z)$ [18, 19]. This strategy has been pursued in [11, 20, 22]. Such an approach is particularly attractive for 1D homogeneous gases: contrary to
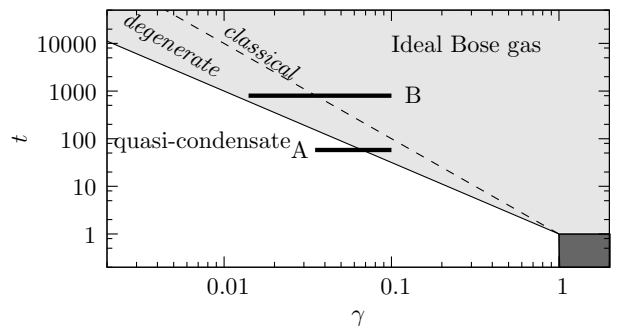

FIG. 1. Phase diagram of the 1D Bose gas in the parameter space (γ, t). The ideal Bose gas to quasi-condensation crossover occurs for $\gamma \simeq \gamma_{co} = t^{-2/3}$ (solid line). Within the ideal Bose gas regime (light gray area), the crossover from the classical to the degenerate sub-regime occurs for $\gamma \simeq \gamma_d = t^{-1/2}$ (dashed line). The region $\gamma, t \gg 1$ (dark gray area) is the fermionised regime. The segments correspond to the regions explored by the two sets of experimental data (see Sec. IV). Note that the effect of quantum fluctuations on the $g^{(1)}$ function in the quasi-condensate regime are noticeable only for extremely low temperature [21], which is experimentally irrelevant.

higher dimensions, no ultraviolet divergence occurs when calculating $g^{(1)}(z)$, so that no energy cut-off is required for this particular quantity. This problem can then be mapped onto a time-independent 2D Schrödinger problem, describing a single particle evolving in imaginary time [18], thus leading to fast and easy-to-implement calculations.

The classical field model is parametrised by a single dimensionless variable $\nu = \gamma/\gamma_{co} = \gamma t^{2/3}$, provided that lengths are rescaled by the correlation length $l_c = \hbar^2 \rho/(m k_B T)$ [18, 23]. Simple analytic formulas are found in the two limits of the ideal Bose gas regime ($\nu \gg 1$) and the quasi-condensate regime ($\nu \ll 1$): the momentum distribution is Lorentzian in both limits, with its full width at half maximum (FWHM) being $\Delta p = 2\hbar/l_c$ in the ideal gas limit and $\Delta p = \hbar/l_c$ in the quasi-condensate limit. One recovers here the expressions derived from the highly degenerate ideal Bose gas model and the high-temperature Bogoliubov theory [17] respectively. Results of numerical calculations spanning the crossover between those two regimes are reported in Fig. 2, where one assumes a fixed value $t = 1000$ and parametrises the system with γ instead of ν. We define the crossover region as the domain for which Δp (shown in Fig. 2(a) as the dashed line), differs by more than 10% from both asymptotic limits ($\hbar/l_c$ and $2\hbar/l_c$), and we find that the crossover extends over about one order of magnitude in ν, or equivalently in γ at fixed t. Looking at the shape of the momentum distribution, we recover the Lorentzian distribution in both asymptotic regimes and, for any value of ν, we find momentum tails decreasing as $1/p^2$, as expected from the analog single-particle problem [24].

C. Validity of the classical field theory at the quasi-condensation crossover

The classical field theory is valid only if the population of the relevant modes is large. Within the ideal Bose gas regime, this requires $\rho \gg \rho_d = \sqrt{mk_BT}/\hbar$, *i.e.* a highly degenerate gas. This condition writes equivalently $\gamma \ll \gamma_d$ where $\gamma_d = t^{-1/2}$ is the interaction parameter at degeneracy. Thus, the classical field theory only correctly describes the quasi-condensation crossover (which occurs at $\gamma \simeq \gamma_{co}$) provided that $\gamma_{co} \ll \gamma_d$. The last condition translates into $t^{1/6} \gg 1$. Since crossovers span typically about one order of magnitude in γ, one requires that $t \gtrsim 10^6$. This value is very difficult to achieve experimentally on cold-atoms experiments while maintaining a temperature sufficiently low to ensure the 1D condition, $k_BT \ll \hbar\omega_\perp$, unless extremely weak atomic interactions are reached, using for instance a Feshbach resonance [25].

In the experiment presented here, we have $t < 1000$. In this case, according to the above argument, the classical field approach is expected to be inaccurate at the quasi-condensation crossover. This can be seen in Fig. 2(a), which shows the FWHM of the momentum distribution as a function of γ according to the ideal Bose gas theory and the classical field prediction for $t = 1000$. The ideal Bose gas theory is parametrised by $\chi = \gamma/\gamma_d \simeq \rho_d/\rho$, which quantifies the level of degeneracy: the FWHM of the momentum distribution within this theory goes from the Maxwell-Boltzmann prediction for $\chi \gg 1$ to $2\hbar/l_c$ for $\chi \ll 1$, and this crossover spans more than one order of magnitude in χ, or equivalently in γ at fixed t. The classical field theory correctly describes the quasi-condensation crossover only if it shares a common plateau with the ideal Bose gas theory at $\Delta p = 2\hbar/l_c$ in the degenerate ideal Bose gas regime, where $\gamma_{co} \ll \gamma \ll \gamma_d$. As seen in Fig. 2(a), this is not the case at all for $t = 1000$: the highly degenerate ideal Bose gas regime is not very well identified for such a small value of t as far as the momentum distribution is concerned, so that the classical field theory does not correctly describe the quasi-condensation crossover.

D. Quantum Monte Carlo approach

For $t < 10^6$, one needs therefore a more accurate treatment than the above-mentioned classical field approximation. We make use of QMC simulations to provide numerically exact results for the Lieb-Liniger model at finite temperature. Bosons in continuous space can be efficiently simulated making use of the density matrix renormalization group in one dimension [26] and Monte Carlo techniques in arbitrary dimensions. Variational and diffusion Monte Carlo results for the first-order correlation function at $T = 0$ are reported in Ref. [27]. At finite temperature, one can in principle make use of path-integral Monte Carlo simulations [28, 29], although we are not aware of explicit calculations for the Lieb-Liniger model.

This latter technique requires the discretization of the imaginary-time dimension (Trotter approximation), and its influence on the simulation results has to be carefully removed. Here, we adopt a rather complementary approach, discretizing the spatial dimension instead [26]. Indeed, bosonic lattice models lend themselves to efficient QMC simulations free of any Trotter approximation. By discretizing the field operator $\hat{\psi}^{(\dagger)}(z) \approx \hat{b}_j^{(\dagger)}/\sqrt{a}$, where a is the lattice spacing, $\hat{b}_j$, $\hat{b}_j^\dagger$ are bosonic operators at site j, and $z \approx ja$, we obtain the Bose-Hubbard Hamiltonian

$$\hat{H}_{\text{BH}} = \sum_j \Big[-J\left(\hat{b}_{j+1}^\dagger \hat{b}_j + \text{h.c.}\right) + \frac{U}{2}\hat{n}_j(\hat{n}_j - 1) \\ -(\tilde{\mu} - v_j)\,\hat{n}_j \Big], \tag{2}$$

with $\hat{n}_j = \hat{b}_j^\dagger \hat{b}_j$, and parameters $J = \hbar^2/(2ma^2)$, $U = g/a$, $\tilde{\mu} = \mu - 2J$. We also include the presence of an external potential $V(z)$, discretized to give v_j. The Lieb-Liniger parameters γ and t read

$$\gamma = \frac{U}{2Jn} \;, \quad \text{and} \quad t = \frac{4k_BT}{J}\left(\frac{J}{U}\right)^2, \tag{3}$$

where $n = \langle \hat{n}_j \rangle = \rho a$ is the lattice filling.

We study the Bose-Hubbard approximation to the Lieb-Liniger Hamiltonian by making use of Stochastic Series Expansion (SSE) QMC [30, 31], extensively used to investigate lattice bosons. The Lieb-Liniger model is correctly recovered when the lattice spacing is much smaller than the correlation length in the system. In the classical ideal Bose gas regime, this condition amounts to require $\lambda_{\text{dB}}/a = \sqrt{4\pi J/(k_BT)} \gg 1$. On the other hand, in the degenerate ideal Bose gas regime and quasi-condensate regime, we need $l_c/a \gg 1$, implying $2J/(U\gamma t) \gg 1$ and $4J/(U\gamma t) \gg 1$ respectively. The first-order correlation function and the momentum distribution are efficiently sampled with SSE-QMC during the directed-loop update [30, 31]. The lattice simulation reproduces faithfully the momentum distribution of the Lieb-Liniger model for momentum $p \ll \hbar\pi/a$.

Fig. 2 shows QMC calculations for a homogeneous gas at $t = 1000$, for values of γ that span the quasi-condensation crossover. In Fig. 2(a) the FWHM of the momentum distribution calculated with QMC is compared to that of the classical field and of the ideal Bose gas models. The QMC results follow the ideal Bose gas prediction almost until the FWHM of the ideal Bose gas prediction crosses that of the classical field prediction at $\gamma = \gamma_c$, and then converges towards the classical field prediction. The disagreement between QMC and the above theories never exceeds 20%. These results mitigate the "failure" of the classical field approximation: as long as the FWHM is concerned, an approximate model where one uses the ideal Bose gas prediction for $\gamma > \gamma_c$ and the classical field prediction for $\gamma < \gamma_c$, would give the correct predictions within 20% error. Investigation of the full momentum distribution is shown in Fig. 2(b) for
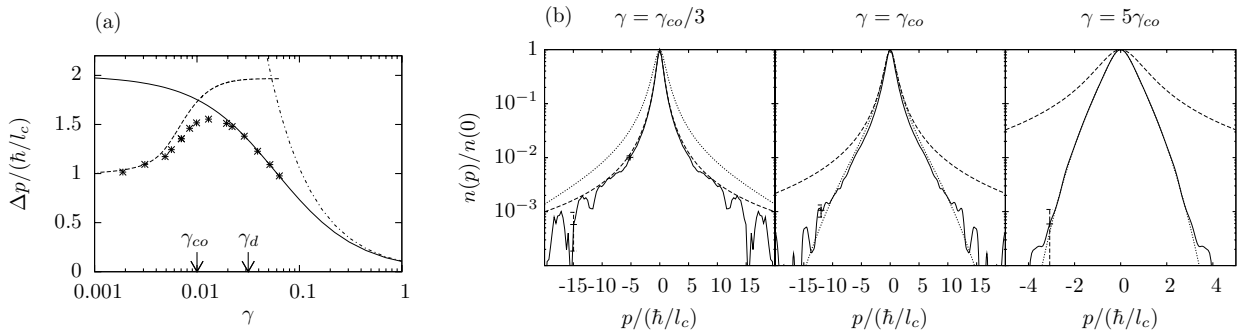
FIG. 2. Momentum distribution of a homogeneous gas at a $t = 1000$. (a) FWHM according to the classical field theory (dashed line), ideal Bose gas theory (solid line), Maxwell-Boltzmann prediction (dash-dotted line) and QMC calculations (stars). The arrows show the interaction parameter at the quasi-condensation crossover ($\gamma_{co} = t^{-2/3}$) and at the degeneracy crossover ($\gamma_d = t^{-1/2}$). (b) momentum distribution in log scale for three different value of γ. Shown are QMC results (solid lines), classical field predictions (dashed lines) and ideal Bose gas prediction (dotted lines). Error bars, shown for a single point on the side of the profile, corresponds to one standart deviation of the QMC calculation.

three different values of γ. On the ideal Bose gas side of the quasi-condensation crossover, for $\gamma = 5\gamma_{co}$, the QMC momentum distribution follows closely the ideal Bose gas behaviour. The classical field result is recovered for $\gamma \approx \gamma_{co}/3$, while the momentum width is still about 10% above the Bogoliubov prediction. For $\gamma = \gamma_{co}$, we find that the tails of the momentum distribution agree well with the ideal Bose gas prediction, while the width of the distribution is narrowed by about 20%. Finally, note that, although the highly degenerate ideal Bose gas prediction $\Delta p = 2\hbar/l_c$ has not been reached before the gas undergoes the quasi-condensation crossover, the momentum distribution at $\gamma \simeq \gamma_{co}$ is much narrower than the Maxwell-Boltzmann prediction (dash-dotted line in Fig. 2(a)), so that the effect of degeneracy within the ideal Bose gas regime is already substantial.

E. Local density approximation

While the previous results hold for homogeneous infinite systems, in the experiment described below, the gas is trapped longitudinally in a harmonic confinement of frequency $\omega/(2\pi)$. As long as the correlation length l_c is much smaller than the cloud size L, however, a local density approximation (LDA) is valid: at a given position z, the local value of an observable O is that of a homogeneous gas ($O_{\rm hom}$) at the chemical potential $\mu_{\rm loc}(z) = \mu - m\omega^2 z^2/2$, and the global value for a trapped system ($O_{\rm trap}$) can be obtained by adding the contributions of each slice of the gas, i.e.,

$$O_{\rm trap}(\omega, \mu) = \sqrt{\frac{2}{m\omega^2}} \int_0^\infty \frac{d\tilde{\mu}}{\sqrt{\tilde{\mu}}} \, O_{\rm hom}(\mu - \tilde{\mu}) \, . \quad (4)$$

Therefore, within this approximation and for a given value of μ (fixing the peak density), the normalized momentum distribution is independent of ω, while the total atom number scales as $1/\omega$. For a gas whose peak linear density lies in the crossover from the degenerate ideal

Bose gas regime to the quasi-condensate regime, the LDA condition $l_c \ll L$ writes $\omega \ll \left(mg^2 k_B^2 T^2/\hbar^5\right)^{1/3}$ [25]. At much higher densities, when almost the whole cloud lies within the quasi-condensate regime, the LDA condition gives $\omega \ll k_B T\sqrt{2mg/\rho}/\hbar^2$ [8]. Both conditions are fulfilled in the data shown below, so that the LDA is expected to be valid. Using QMC, we compute the momentum distribution (normalised to the total atom number) of a harmonically trapped gas for different chemical potentials (i.e. different peak linear densities) and temperatures. To shorten the computational time, calculations are performed for trapping frequencies five times larger than the experimental values, while still satisfying the LDA condition, as verified numerically. The computed momentum distribution are multiplied by five to be compared to experimental data. Linear interpolation between the calculated distributions permits the calculation of the momentum distribution for any chemical potential μ and temperature T, and enables us to perform fits to the measured distribution. We check a posteriori that the interpolation is correct up to a few percent.

III. EXPERIMENTAL TECHNIQUES

One-dimensional atomic clouds are realised in our experiment using an atom-chip setup [32]. More specifically, we load 8×10^4 Rb^{87} atoms in the modulated guide described in [3]. The longitudinal harmonic potential has an oscillation frequency of about 8 Hz and is obtained by DC currents running through wires I_3 and I_4 (see Fig. 3). The transverse potential is provided by three wires carrying a 200 kHz sinusoidal current. The transverse oscillation frequency can be varied from a few hundred Hz to tens of kHz by changing the current amplitude. An important feature of this design is the independence between the longitudinal and transverse confinements. After 1200 ms of radio-frequency evaporation, we let the
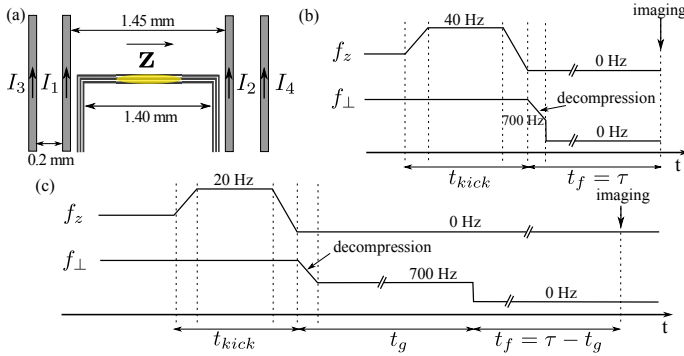
FIG. 3. (a) Wire configuration: currents I_1, I_2, I_3 and I_4 realise the longitudinal trapping potential of frequency f_z. The transverse confinement of frequency $f_\perp$ is ensured by the three wires carrying a current modulated at 200 kHz. (b,c) Focusing sequences. The focusing potential, harmonic to order 5 in z, is applied during t_{kick} before the longitudinal potential is turned off. After a free evolution during the focusing time τ, an absorption image is taken. Without guiding, see (b), the transverse confinement is removed during the whole focusing time, though a 1 ms ramp down to $f_\perp = 700$ Hz is carried out to decrease the transverse expansion. In the presence of guiding, see (c), $f_\perp$ is kept at 700 Hz for a time t_g, during which the cloud does not fall. Numerical values in (b) and (c) correspond to data of Fig. 5 and 4 respectively.

cloud reach thermal equilibrium for 400 ms, after which no remaining breathing can be observed. To characterise the atomic cloud, we perform *in situ* density fluctuations measurements, analysing the noise in an ensemble of absorption images as described in [5].

To measure the momentum distribution, one can monitor the free expansion of the gas after all confining potentials have been turned off. The rapid transverse expansion amounts to an effective instantaneous suppression of the interactions, so that the longitudinal expansion reflects faithfully the initial momentum distribution in the trap. However, reaching the far field regime where the longitudinal density profile is homothetic to the momentum distribution requires unrealistically large field of view and long expansion time for our experimental parameters. We thus use the so called focusing technique, already applied to 1D [11, 33, 34] and 2D systems [35]. Its principle is described below. A strong longitudinal harmonic potential is applied for a very short time during which atoms do not have time to move but acquire a longitudinal momentum shift $\delta p = -Az$, proportional to their distance z to the trap center. Then, the atomic interactions are suppressed by switching off the transverse confinement, and the longitudinal confinement is removed so that the cloud starts a free evolution. After a focusing time $\tau = m/A$, the longitudinal density distribution $f(z)$ is homothetic to the initial momentum distribution $n(p) = (m/\tau)f(p\tau/m)$ [36]. More precisely, the time sequence we use is drawn in Fig. 3. The longitudinal focusing potential is realized by a four-wire configuration that cancels out the non harmonic terms up to the 6th

order, thus minimizing aberrations. It has an oscillation frequency $\omega_{\text{kick}}/2\pi = 40$ Hz and it is applied for about $t_{\text{kick}} = 0.6$ ms. After the focusing pulse, we ramp the transverse frequency down to 700 Hz in 1 ms before completely turning off the transverse trapping potentials and letting the cloud evolve freely. The 1 ms transverse ramp is used to limit the transverse velocity spread, so that the transverse final expansion of the cloud is reduced and the signal to noise ratio (SNR) is increased. We verified that this ramp is however quick enough to leave the longitudinal velocity distribution unchanged. After free evolution during the focusing time $\tau \simeq 1/\omega_{\text{kick}}^2 t_{\text{kick}} \approx 27$ ms, we take an absorption image of the cloud and extract the longitudinal density distribution, from which we deduce the initial momentum distribution. The focusing time τ is adjusted by minimising the width of the density distribution of cold samples. Moreover, the width of very cold clouds saturates at a value that gives us the momentum resolution $\Delta p/\hbar = 0.2$ μm^{-1}. This resolution is significantly smaller than the width of the data in Fig. 5.

On the other hand, a better resolution may be necessary for a momentum distribution that is much narrower. This can be achieved by a longer focusing time τ. However, the depth of field of our optical system limits the maximum free fall under gravity to about 3 mm, corresponding to a free fall time of about 25 ms. Nevertheless, larger focusing times can be obtained if a transverse potential is maintained during the focusing time, strong enough to overcome gravity (which acts in the transverse plane in our experiment), but weak enough so that atomic interactions are negligible. More precisely the guiding scheme we use is the following. After having performed the longitudinal focusing pulse and switched off the longitudinal potential, we ramp the transverse frequency down in 1 ms, similar to the procedure described before. The final transverse frequency is $f_l = 700$ Hz, which is the lowest value that allows the atoms to remain transversally trapped. We then hold the cloud for a guiding time t_g, at the end of which we switch off the transverse confinement and let the cloud fall freely for t_f. The guiding does not affect the longitudinal free evolution as long as the effect of interactions stays negligible. We have checked that this is indeed the case for the explored parameter range by measuring the longitudinal density profile at focus $f(z)$ of identical clouds, either without guiding and a focusing time $\tau = t_f = 24.7$ ms, or with the above guiding scheme and $\tau = t_g + t_f = 43.3$ ms, where $t_g = 20.6$ ms and $t_f = 22.7$ ms. The functions $f(mz/\tau)$, shown on Fig. 4 for a cloud of 7000 atoms at $T \approx 95$ nK, give indeed the same momentum distribution. The validation of this technique paves the way towards high resolution measurements of momentum distribution of 1D gases.
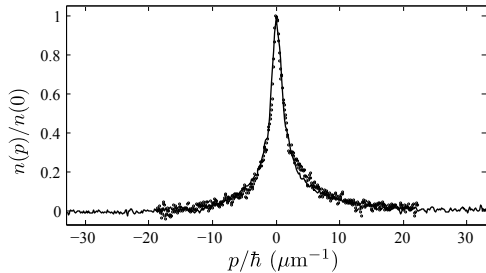
FIG. 4. Momentum distribution of a gas of about 7000 atoms at thermal equilibrium, in a 7.5 Hz longitudinal trap, and 4.6 kHz transverse trap. The solid distribution is obtained without guiding and with a free fall of 24.7 ms. The circles are the momentum distribution of the same sample, but with a guiding time of 20.6 ms followed by a free fall of 22.7 ms.

IV. EXPERIMENTAL RESULTS

Fig. 5 shows experimental results referring to two different parameter sets (particle number, temperature and trapping potential). In both cases, the momentum distribution is obtained without the guiding scheme, with a focusing time of 27 ms.

A. On the quasi-condensate side of the crossover

Data in Fig. 5(A) correspond to a cloud initially trapped with a transverse oscillation frequency $\omega_\perp/(2\pi) = 6.4$ kHz and a longitudinal frequency of 8.3 Hz, measured using parametric heating and dipole oscillations respectively. Since the cloud temperature and chemical potential are much smaller than the transverse level spacing, the system is well described by a 1D gas with a coupling constant $g = 2\hbar\omega_\perp a_s$, where $a_s = 5.3$ nm is the 3D scattering length [37]. In Fig. 5 (A,1-2), we show the measured momentum distribution (points) with a QMC fit (solid lines) that yields $T = 72$ nK, corresponding to $t = 76$. Note that the shape is reproduced up to a few per cent. We report in Fig. 1 the segment $[(\gamma_m, t), (\gamma_M, t)]$ corresponding to the domain explored by the data: γ_m corresponds to the peak density, and the segment length is such that 80% of the atoms lie in a region of density larger than that associated to γ_M. We find that $\gamma_m \simeq \gamma_{co}/2$, where $\gamma_{co} = t^{-2/3}$ is the interaction parameter at the quasi-condensation crossover. Thus the cloud lies quite deeply in the quasi-condensate regime. However, the measured momentum distribution is substantially broader than that predicted using the quasi-condensate Lorentzian $n(p) \propto 1/(p^2 + (\hbar/l_c)^2)$ together with the LDA, shown as the dashed line in Fig. 5(A,1). On the other hand, for such a value of γ_m, the momentum distribution shows slowly decreasing tails, compatible with a Lorentzian behavior within a few percent in a wide range of momenta. This is seen in Fig. 5(A,2) where the dashed-dotted line shows a $1/p^2$ decrease. For our SNR of about 80, data are compatible with a Lorentzian
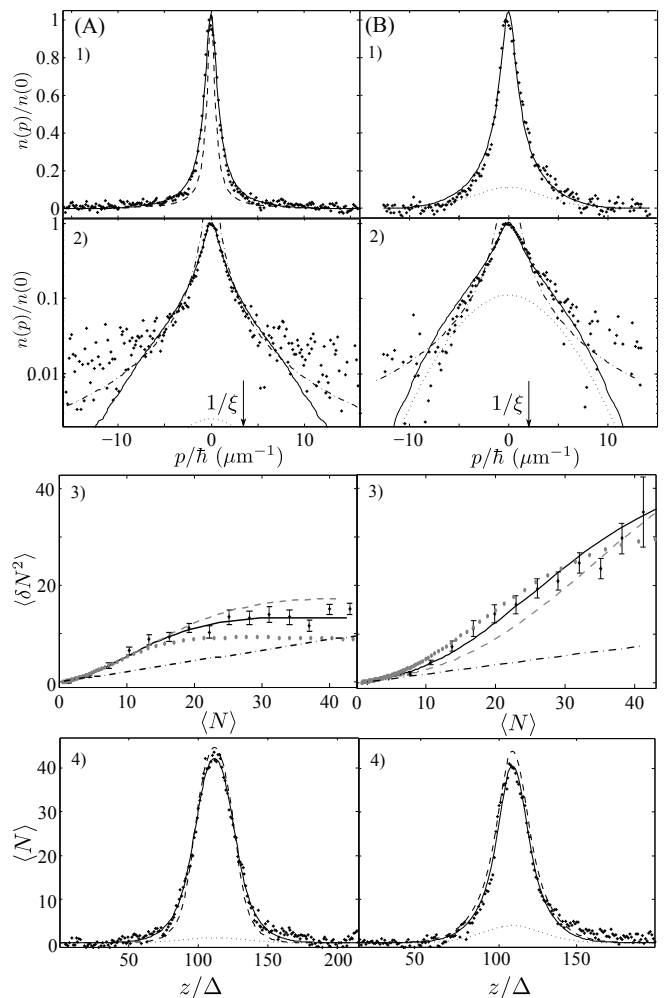

FIG. 5. Data for atoms confined in a harmonic trap of transverse oscillation frequency of (A) 6.4 kHz and (B) 2.1 kHz, and a longitudinal oscillation frequency of (A) 8.3 Hz and (B) 7.6 Hz. The pixel size, in the object plane, for *in situ* data is $\Delta = 2.7\ \mu$m. 1),2) momentum distribution in linear and log scales. QMC fits are shown in solid lines, yielding (A) $T = 72$ nK and (B) $T = 84$ nK. The dashed line in (A,1) is the prediction using the LDA and the Lorentzian momentum distribution in the quasi-condensate limit. In 2), the dashed-dotted lines give the $1/p^2$ behavior, while the momentum associated with the healing length $\xi = \hbar/\sqrt{m\rho g}$ indicates that sample (A) is more in the quasi-condensate, with $\Delta p \ll \hbar/\xi$, and sample (B) is more in the ideal Bose gas, with $\Delta p \gg \hbar/\xi$. In addition, the dotted lines indicate the contribution from the transverse excited states, which is insignificant for data (A) and hence neglected in our analysis. 3) *in situ* density fluctuations, with Yang-Yang prediction in solid lines, evaluated at the above-mentioned temperatures. The gray dashed and dotted lines shows Yang-Yang predictions with 30% temperature deviations. The dash-dotted lines indicate the poissonian fluctuation level. 4) *in situ* profile, with the QMC profile in dashed lines. The dotted lines again show the contribution from transverse excited states. We also plot in solid lines the density profile fitted with Yang-Yang calculation, which yields (A) $T = 111$ nK and (B) $T = 76$ nK.

behavior at large p.

As shown in [3, 6], an independent and reliable thermometry can be carried out using *in situ* density fluctuations, provided the pixel size Δ is both much larger than the correlation length of density fluctuations, and much smaller than the typical length scale of the variation of the mean density profile : the atom number fluctuations are then given by the thermodynamic relation $\langle \delta N^2 \rangle = k_B T \Delta \partial \rho / \partial \mu$, where $\rho(\mu, T)$ is the equation of state of homogeneous 1D gases, known exactly using the Yang-Yang calculation [6], and the derivative is computed for μ such that $\rho(\mu, T) = \langle N \rangle / \Delta$ is the local density. The above criterion is well fulfilled in our experiment and the measured density fluctuations are shown in Fig. 5(A,3). For linear densities larger than 25 atoms per pixel, fluctuations are almost independent of the density, which confirms that the center part of the gas lies within the quasi-condensate regime. Indeed, in this regime $\mu \simeq g\rho$, so that the thermodynamic relation reduces to $\langle \delta N^2 \rangle = \Delta k_B T / g$, which does not depend on $\langle N \rangle$. The fluctuations computed using the thermodynamic relation and the Yang-Yang equation of state, for the temperature $T = 72$ nK (obtained by fitting the momentum distribution with the QMC results) are shown as solid line. The data are in agreement with this prediction. With our SNR, the density fluctuations based thermometry has a precision of about 20% (see gray curves in Fig. 5(A,3)), less precise than the thermometry obtained by fitting QMC calculations to the momentum distribution.

Finally, we compare in Fig. 5(A,4) the measured *in situ* density profile to the QMC density profile (within LDA) for $T = 72$ nK (dashed line). We find a good agreement for most of the profile, although the measured data show higher wings. Since the central part of the cloud lies deep in the quasi-condensate regime, a large part of the cloud follows the Thomas-Fermi profile, and all the information on the temperature lies in the *small* wings. This renders Yang-Yang thermometry based on density profile less precise and extremely sensitive to the shape of the wings. Here, a Yang-Yang fit to the density profile gives $T = 110$ nK, a value 40% higher than that extracted from the QMC fit, incompatible with the measured momentum distribution or the density fluctuation measurements. This discrepancy, and thus the presence of the inflated wings, may come from the anharmonicity of the potential due to its residual roughness [38]. Alternatively, it may also indicate a lack of perfect thermal equilibrium.

B. On the ideal Bose gas side of the crossover

While the previous results probe mainly the quasi-condensate regime, we also probe the ideal Bose gas side of the quasi-condensation crossover, *i.e.* data with $\gamma_m > \gamma_{co} = t^{-2/3}$. The ideal Bose gas regime shows a very different behaviour from the trivial Maxwell-Boltzmann prediction only for a large t parameter, for which the quasi-condensation crossover occurs for an already highly degenerate gas. If one wishes to preserve the 1D condition $k_B T \ll \hbar\omega_\perp$, large t parameters can be accessed only by decreasing the transverse confinement [25]. We thus reduced the transverse confinement to 2.1 kHz. Data are shown in Fig. 5(B). No saturation of the density fluctuations is seen on the *in situ* fluctuation measurements, which indicates that the gas does not lie in the quasi-condensate regime. Fluctuations however rise well above the poissonian level (shown as dashed-dotted line on Fig. 5(B,3)) so that the gas is highly degenerate. Contrary to the data of Fig. 5(A), we now have $k_B T / (\hbar\omega_\perp) = 0.8$ which is of the order of unity, so that the transverse excited states contribute to the measured fluctuations and momentum distribution. We take into account the population of transverse excited states, assuming that they behave as independent ideal 1D Bose gases, while the transverse ground state is treated as a Lieb-Liniger gas. This modified Lieb-Liniger model has been used with success to describe density profiles [4] and density fluctuations [6], and has been applied to predict the rms width of momentum distribution [11]. Here we use our QMC calculations to describe the transverse ground state. A fit using the above strategy reproduces well the measured momentum distribution (see Fig. 5(B,1)), and yields the temperature $T = 84$ nK, corresponding to $t = 840$. The segment in the phase space (γ, t) explored by the data is shown in Fig. 1: the peak linear density is close to the quasi-condensation crossover density and most of the cloud lies in the degenerate ideal Bose gas regime. The contribution of the excited states to the momentum distribution is seen in Fig. 5(B,1): it is only 10% in the center but it rises to almost 50% in the wings around $|p|/\hbar \simeq 5$ μm^{-1}. Fig. 5(B,2) shows that the theoretical momentum distribution decreases faster than $1/p^2$ at large momenta. This is mainly due to the contribution of the excited states, which have approximately Gaussian momentum tails. However, with our SNR of about 50, no deviation from a $1/p^2$ behavior can be identified. We report in Fig. 5(B,2) the fluctuations expected for the temperature $T = 84$ nK (obtained from the fit of the momentum distribution with QMC). They are in agreement with the measured fluctuations. Note however that, for these parameters, the uncertainty of thermometry based on fluctuations is about 30% (see gray lines in Fig. 5(B,3)). The density profile expected for $T = 84$ nK is not far from the measured one (see Fig. 5(B,4)). In contrast to case (A), Yang-Yang thermometry based on the profile is less sensitive to tiny modifications of the wings, since the profile of the high-density regions is also affected by the temperature. Thus, a thermometry based on the profile is expected to be quite precise and the potential roughness is expected to have a smaller effect. A Yang-Yang fit to the experimental profile yields a temperature of 76 nK, different only by 10% from the temperature deduced from the momentum distribution.

V. CONCLUSIONS AND PROSPECTIVES

We have shown that for $t < 10^6$, a simple 1D classical field approximation where the momentum distribution is computed without energy cutoff, fails to describe the momentum distribution of weakly interacting 1D Bose gases in the crossover from ideal Bose gas to quasi-condensate. Thus, we performed QMC calculations to investigate the crossover. Experimentally, we measure the momentum distribution with the focusing technique, which is improved by a guiding scheme for enhanced resolution. We show that the temperature deduced from the momentum distribution is in agreement with an independent fluctuation-based thermometry. We find that the result of Bogoliubov theory is not appropriate for parameters that are close to the ones relevant to this article, even when the cloud lies quite deeply in the quasi-condensate regime. In [11], it has been proposed to use the mean kinetic energy deduced from measured momentum distribution in order to extract the temperature using the modified Yang-Yang calculation. For the data presented in this article, with a SNR of about 50, the measured momentum distribution shows tails compatible with a $1/p^2$ behavior both in the quasi-condensate regime and in the degenerate ideal Bose gas regime. Therefore, extraction of the mean kinetic energy from the data is impossible. We argue that this technique was applicable in [11] because of the more 3D nature of the gas: for quasi 1D gases, as discussed in section IV B, the contribution of the transverse excited states leads to fast decaying tails, which enable the extraction of the mean kinetic energy per particle. We also remark that neither our measurements nor the QMC calculations display the asymptotic behaviour of $1/p^4$, which only appears at even larger momenta for our parameters. On the other hand, we believe that this behaviour could be more readily discernable in the strongly interacting regime, where the $1/p^4$ tail should contain a larger proportion of the atoms.

This work opens many perspectives for the study of 1D gases. First of all, we show that momentum distribution measurements provide a precise thermometry for 1D Bose gases. While in this article we use QMC calculations to fit the temperature of experimental data, a rough estimate of the cloud temperature could be performed with a lower numerical cost. Indeed, the comparison with the exact QMC momentum distribution shows that a model which combines the ideal Bose gas theory and the classical field approximation gives the correct width within 20% precision. Second, momentum distribution measurements are essential to characterize more complex systems. For instance, in the presence of a lattice, it enables the investigation of the correlation properties at the Mott and/or pinning transitions. Contrary to Bragg spectroscopy [10, 14], where a single momentum component is probed at each shot, the focusing method as well as time of flight method gives access to the whole distribution at the same time, which allows for noise correlation measurements in momentum space [23, 39]. Finally, recording the time evolution of the momentum distribution is essential to monitor the non-equilibrium dynamics and address the issue of thermalization in 1D closed quantum systems. For example, the dynamics resulting from a quench of the 1D coupling constant can be investigated. The measure of the momentum distribution of impurities would also permit the study of impurity dynamics, which is currently under intense investigation [40].

[1] Z. Hadzibabic *et al.*, Nature **441**, 1118 (2006).
[2] M. Greiner *et al.*, Nature **415**, 39 (2002).
[3] T. Jacqmin, J. Armijo, T. Berrada, K. V. Kheruntsyan, and I. Bouchoule, Phys. Rev. Lett. **106**, 230405 (2011).
[4] A. H. van Amerongen, J. J. P. van Es, P. Wicke, K. V. Kheruntsyan, N. J. van Druten, Phys. Rev. Lett. **100**, 090402 (2008).
[5] J. Armijo, T. Jacqmin, K. V. Kheruntsyan, and I. Bouchoule, Phys. Rev. Lett. **105**, 230402 (2010).
[6] J. Armijo, T. Jacqmin, K. .V. Kheruntsyan, and I. Bouchoule, Phys. Rev. A **83**, 021605(R) (2011).
[7] C. N. Yang and C. P. Yang, J. Math. Phys. **10**, 1115 (1969).
[8] F. Gerbier *et al.*, Phys. Rev. A **67**, 051602 (2003).
[9] M. Hugbart *et al.*, The European Physical Journal D **35**,

155 (2005).
[10] S. Richard *et al.*, Phys. Rev. Lett. **91**, 010405 (2003).
[11] M. J. Davis, P. B. Blakie, A. H. van Amerongen, N. J. van Druten, and K. V. Kheruntsyan, Phys. Rev. A **85**, 031604 (2012).
[12] S. Dettmer *et al.*, Phys. Rev. Lett. **87**, 160406 (2001).
[13] S. Manz *et al.*, Phys. Rev. A **81**, 031610 (2010).
[14] N. Fabbri, D. Clément, L. Fallani, C. Fort, M. Inguscio, Phys. Rev. A **83**, 031604 (2011).
[15] M. Olshanii and V. Dunjko, Phys. Rev. Lett. **91**, 090401 (2003).
[16] A. Minguzzi, Physics Letters A **294**, 222 (2002).
[17] C. Mora and Y. Castin, Phys. Rev. A **67**, 053615 (2003).
[18] Y. Castin *et al.*, J. of Mod. Optics **47**, 2671 (2000).
[19] Y. Castin, J. Phys IV **116**, 87 (2004).

[20] D. Gallucci, S. P. Cockburn, and N. P. Proukakis, arXiv: 1205.6075 .

[21] Quantum fluctuations lead to an algebraic decay of $g^{(1)}$ as $(z/\xi)^{-\sqrt{\gamma}/2\pi}$ for distances $\xi < z < \hbar^2/(mk_BT\xi)$, where $\xi = \hbar/\sqrt{m\rho g}$ is the healing length. For the decay to be noticeable over this range, one requires $k_BT \propto \rho g \exp(-2\pi/\sqrt{\gamma})$.

[22] S. P. Cockburn, D. Gallucci, and N. P. Proukakis, Phys. Rev. A **84**, 023613 (2011).

[23] I. Bouchoule, M. Arzamasovs, K. V. Kheruntsyan, and D. M. Gangardt, Accepted in Phys. Rev. A (2012).

[24] In terms of the analog quantum problem, $g^{(1)}(z) = \Sigma_j A_j e^{-(\epsilon_j-\epsilon_0)|z|}$, where the sum is carried out over the eigenstates of energy ϵ_j, and the factors A_j are obtained by wavefunction overlaps. The Fourier transform is a sum of Lorentzian, which shows $1/p^2$ tails (uniform convergence is ensured by the fast decay of the A_j's at large energy).

[25] I. Bouchoule, K. V. Kheruntsyan, and G. V. Shlyapnikov, Phys. Rev. A **75**, 031606 (2007).

[26] B. Schmidt and M. Fleischhauer, Phys. Rev. A **75**, 021601 (2007).

[27] G. E. Astrakharchik and S. Giorgini, Phys. Rev. A **68**, 031602 (2003).

[28] D. M. Ceperley, Rev. Mod. Phys. **67**, 279 (1995).

[29] M. Boninsegni, N. V. Prokof'ev, and B. V. Svistunov, Phys. Rev. E **74**, 036701 (2006).

[30] O. F. Syljuåsen, Phys. Rev. E **67**, 046701 (2003).

[31] A. W. Sandvik, AIP Conf.Proc. **1297**, 135 (2010).

[32] J. Reichel and V. Vuletic, Atom Chips (Wiley-VCH Verlag GmbH, ADDRESS, 2011).

[33] I. Shvarchuck *et al.*, Phys. Rev. Lett. **89**, 270404 (2002).

[34] J. J. P. van Es *et al.*, Journal of Physics B: Atomic, Molecular and Optical Physics **43**, 155002 (2010).

[35] S. Tung, G. Lamporesi, D. Lobser, L. Xia, and E. A. Cornell, Phys. Rev. Lett. **105**, 230408 (2010), in this experiment, a somehow different technique is employed, where a harmonic potential is kept during the focusing.

[36] This relation is easily established using the Wigner function representation, since its evolution under a harmonic potential and its free evolution are those of a classical distribution.

[37] M. Olshanii, Phys. Rev. Lett. **81**, 938 (1998).

[38] Deviations from the harmonic potential by about 30 nK is sufficient to explain the presence of those wings. This value is consistent with the residual roughness we estimated from the measured density variations of very elongated quasi-condensates confined in a longitudinal quartic potential.

[39] S. Fölling *et al.*, Nature **434**, 481 (2005).

[40] J. Catani *et al.*, Physical Review A **85**, 023623 (2012).